Electronic supplementary information (ESI)

Copper doped TiO_2 nanoparticles characterized by X-ray absorption spectroscopy, total scattering, and powder diffraction - a benchmark structure-property study

Nina Lock,[a,b] Ellen M. L. Jensen,[a] Jianli Mi,[a] Aref Mamakhel,[a] Katarina Norén,[c] Meng Qingbo,[d] Bo B. Iversen[a]*

[a]Center for Materials Crystallography, Department of Chemistry and iNANO, DK-8000 Aarhus C, Denmark

[b]Present address: Faculty of Chemistry, Georg-August-Universität Göttingen, D-37077 Göttingen, Germany

[c]MAX IV Laboratory, Lund University, SE-221 00 Lund, Sweden

[d] Key Laboratory for Renewable Energy, Institute of Physics, Chinese Academy of Sciences, Beijing 100190, PR China

*Corresponding author: bo@chem.au.dk

Information provided herein supports experimental details and conclusions drawn in the manuscript.

Powder Diffraction at I711 at the MAX IV Laboratory

Data were collected at beamline I711 at the MAX IV Laboratory, Sweden, using a wavelength of 0.94 Å. The diffracted X-ray patterns were collected on a MAR CCD detector, and the sample-to-detector distance and wavelength were calibrated using a LaB_6 standard from NIST.

Data were integrated in Fit2D[1] and refined in the Fullprof program.[2] The background was described by linear interpolation of refinable points, and a Thompson-Cox-Hastings pseudo-Voigt function was used to describe the peak profiles. The unit cell for silicon was refined on a pure silicon sample and fixed in the refinement of the mixed TiO_2-Si samples. The zero-point was refined along with a transparency parameter and the TiO_2 unit cell. The nanoparticle profiles were described by the Gaussian *W* and Lorentzian *Y* parameters, which were used for size determination after correction for instrument broadening. The refined powder patterns for the TiO_2 and Cu-TiO_2 samples mixed with silicon are shown in Figure S1. The good fits reveal that a spherical model describes the particle morphology satisfactorily. The *R*-values and TiO_2/Si weight ratios determined by the refinement are shown in Table S1.

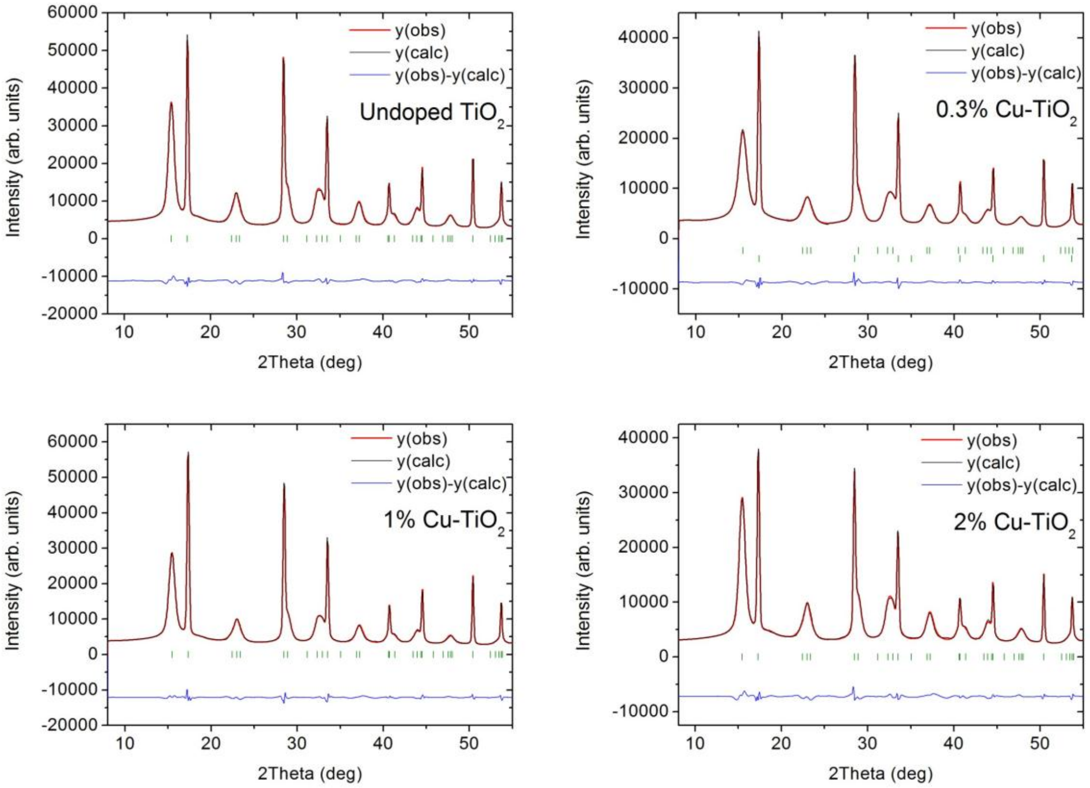

Figure S1. Rietveld refined powder diffraction data collected on nanocrystalline TiO_2 samples mixed with a NIST silicon standard.

Refinement of TiO_2/Si mixtures			
Sample	R_F (%)	R_B (%)	Weight fraction (%)
Undoped TiO_2	1.36	2.08	34.5(3)
Si (in undoped TiO_2)	0.678	1.39	65.5(6)
0.3% Cu-TiO_2	0.592	0.873	67.2(7)
Si (in 0.3% Cu-TiO_2)	1.78	1.09	32.8(3)
1% Cu-TiO_2	0.826	1.22	60.2(7)
Si (in 1% Cu-TiO_2)	0.650	1.10	39.8(3)
2% Cu-TiO_2	1.12	1.85	69.3(8)
Si (in 2% Cu-TiO_2)	0.555	1.16	30.7(3)

Table S1. Refinement *R*-values and weight fractions of TiO_2 and Si determined by the refinements. The weight fractions are used for crystallinity determination (see below).

Determination of the Crystallinity of TiO_2 from Powder Diffraction Data.

The crystallinity, *i.e.* the average weight fraction of the particles that attains the anatase crystal structure, was determined from the Rietveld refinements. The refinements provide the *actual* TiO_2/Si mass ratio (*i.e.* the ratio between crystalline TiO_2 and Si). Since the mass ratio of the TiO_2 and Si powders is known from the preparation of the powder diffraction samples (by simple weighing), the crystallinity can be determined as the ratio: $m(TiO_2\text{, crystalline})/m(TiO_2\text{, sample})$ as shown for undoped TiO_2 as follows (assuming 100% crystalline silicon):

$m(TiO_2\text{,sample}) = 32.9$ mg; $m(Si) = 13.2$ mg; $m(\text{total}) = m(TiO_2) + m(Si) = 46.1$ mg

weight fraction(Si, refinement) = 0.345 corresponding to 13.2 mg

weight fraction(TiO_2, refinement) = 0.655

$m(TiO_2\text{, crystalline}) = 13.2\text{ mg}/0.345\cdot 0.655 = 25.1$ mg

$\text{crystallinity}(TiO_2) = m(TiO_2\text{, crystalline})/\ m(TiO_2\text{,sample})\cdot 100\% = 76.2\%$

We estimate that the error on the crystallinity determination is less than 1%.

Size Determination of TiO_2

The particle sizes were calculated from the profile parameters for the intense (101) reflection as follows. The instrument broadening of the diffraction peaks was subtracted by using the NIST Si powder standard that was mixed with the TiO_2 powders. The instrument corrected peak broadening was described as size broadening alone, as size broadening is the dominating contribution to the peak width for small nanoparticles.

The Gaussian width, H_G, and Lorentzian width, H_L, of a diffraction peak at the diffraction angle 2θ can be expressed as follows, where U, V, W, X, and Y are profile parameters:

$H_G^2 = U\tan^2\theta + V\tan\theta + W$

$H_L = Y/\cos\theta + X\tan\theta$

The Gaussian and Lorentzian contributions to the instrument broadening were calculated from these equations by using the profile parameters refined to the Si standard in the sample.

The Gaussian parameter *W* and the Lorentzian parameter *Y* were refined for the TiO_2 phase for the MAX IV Laboratory data, while the other parameters were fixed to zero, which reduces the expressions to:

$H_G^2(\text{sample}) = W$

$H_L(\text{sample}) = Y/\cos\theta$

The Gaussian and Lorentzian contributions from TiO_2 to the peak width were determined as:

$H_G^2(TiO_2) = H_G^2(\text{sample}) - H_G^2(\text{instrument})$

$H_L(TiO_2) = H_L(\text{sample}) - H_L(\text{instrument})$

For a Thompson-Cox-Hastings pseudo-Voigt function, the following numerical expression describe the relation between the Gaussian and Lorentzian contributions and the full peak width at half maximum intensity, FWHM, in degrees:[3]

$$\text{FWHM}=(H_G^5+2.69269\cdot H_G^4H_L+2.42843\cdot H_G^3H_L^2+4.47163\cdot H_G^2H_L^3+0.07842\cdot H_GH_L^4+H_L^5)^{(1/5)}$$

The particle size, *L*, was determined from the FWHM (in radians) using the Scherrer equation:

$$L = (0.9\cdot\lambda)/(\text{FWHM}\cdot\cos\theta)$$

Relation between unit cell size, crystallinity, and particle size

The relations between the unit cell parameters, sample crystallinity, and particle size are shown in Figure S2. In addition to the undoped sample and the three Cu-TiO_2 samples, data for two other samples (Fe-TiO_2 and W-TiO_2), which are iron and tungsten doped TiO_2, respectively, are included in the plots. These samples were synthesized similarly to the copper doped samples, and PXRD data were collected under the same conditions. The results of these refinements are included here to not base conclusions on just four data points.

The data analysis points to decreasing cell parameters with increasing particle size up to particle sizes of 6-7 nm (Figure S2a). At the same time, however, the unit cell appears to increase with increasing crystallinity (Figure S2b). The crystallinity is observed to be largest for the small nanocrystals (Figure S2d).

There is no trend between the cell parameters as a function of dopant concentration in Cu-TiO_2 (Figure S2c).

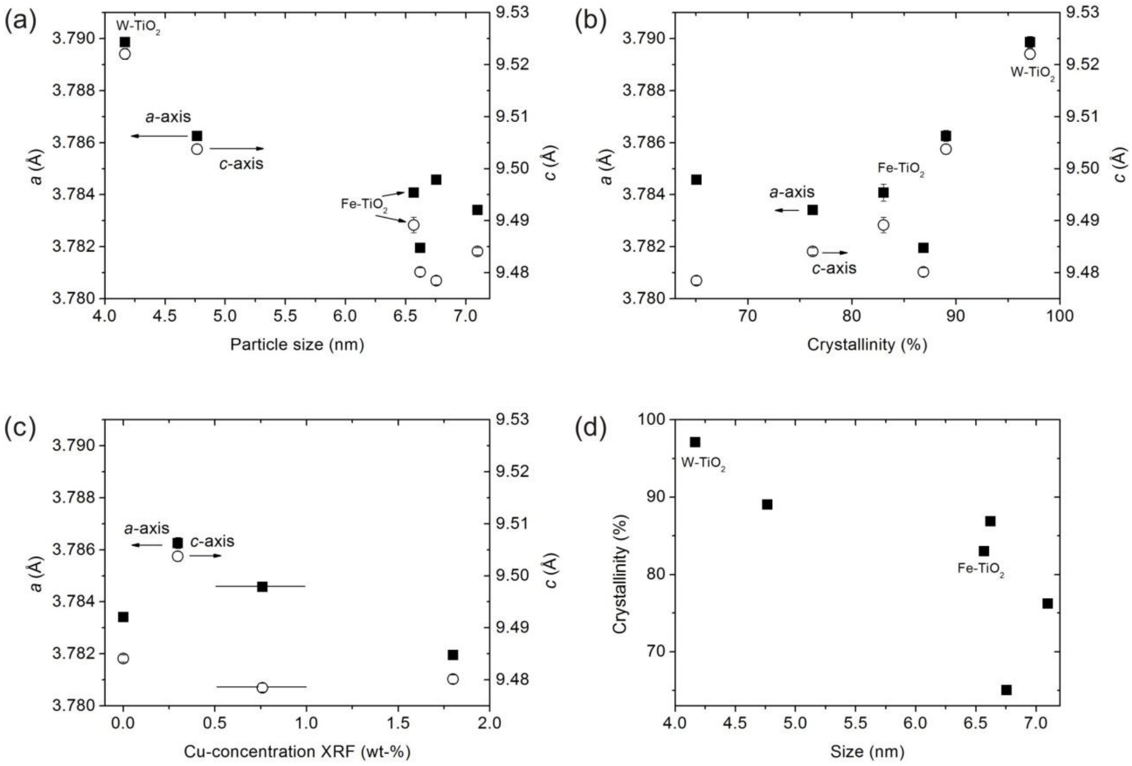

Figure S2. The unit cell parameters, crystallite size, and crystallinity were determined from powder diffraction data for undoped TiO_2, three Cu-TiO_2 samples plus one tungsten doped and one iron doped TiO_2 sample. Here is shown: (a) the unit cell plotted as a function of the particle size, (b) the unit cell as a function of the crystallinity; (c) the unit cell as a function of the copper concentration in Cu-TiO_2 as determined by X-ray fluorescence spectroscopy, and (d) the crystallinity as a function of particle size. The horizontal line in (c) covers the copper concentration from the experimentally determined concentration (lower limit) to the expected concentration (upper limit) for 1% Cu-TiO_2 (see discussion in the section on X-ray fluorescence spectroscopy herein incl. Table S7).

X-Ray Absorption Spectroscopy

X-ray absorption spectroscopy data (XAS) were measured in fluorescence mode at beamline I811 at the MAX IV Laboratory, Sweden, on the undoped and copper doped TiO_2 samples to cover the X-ray absorption near edge structure (XANES) and extended X-ray absorption fine structure (EXAFS) regions. Two or three identical datasets were collected on both the copper- and the titanium absorption *K*-edges (only the titanium edge for the undoped sample).

Data were deglitched by manually removing single sharp outlier points before merging identical datasets in Athena. Theoretical scattering paths were calculated by using the Atoms[4] and feff[5] codes and the Artemis[6] program. The program WinXAS[7] was used to perform data corrections and analysis including background subtraction, data normalization, extraction of the EXAFS signal by cubic splining, Fourier transformation (FT), and data refinement in *R*-space.

Figure S3a displays copper edge XANES data along with copper(I) and copper(II) references to verify that copper is present in Cu-TiO_2 as copper(II). However, Figure S3b shows that one of the samples, 0.3% Cu-TiO_2, was reduced to metallic copper when a pellet of the material was pressed. As discussed in the paper the reduction is most likely caused by presence of isopropanol residues on the particle surface.

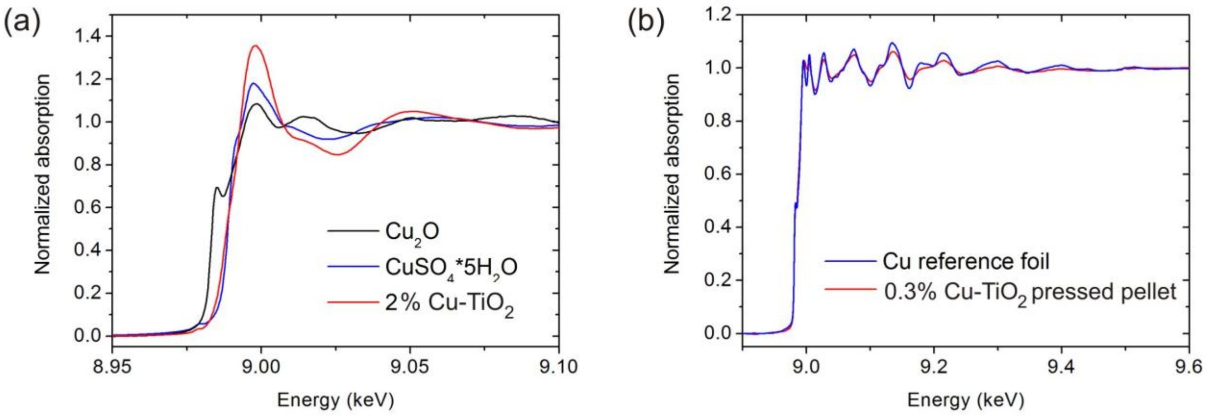

Figure S3. (a) The XANES region of a copper(I) reference (Cu_2O, black), a copper(II) reference ($CuSO_4{\cdot}5H_2O$, blue) and copper edge 2% Cu-TiO_2 data revealing that copper is present as copper(II). (b) Normalized XAS data collected on a pellet of 0.3% Cu-TiO_2 and boron nitride powder plotted along with data collected on a copper reference foil showing that copper was reduced to copper(0) when pressed to a pellet. Data collected on a non-pressed 0.3% Cu-TiO_2 powder is displayed in Figure S4.

Figure S4 shows all datasets as normalized absorption data, *k*-space data, and Fourier transformed data. In Figure S5 Fourier transformed copper- and titanium edge EXAFS data are plotted together for comparison.

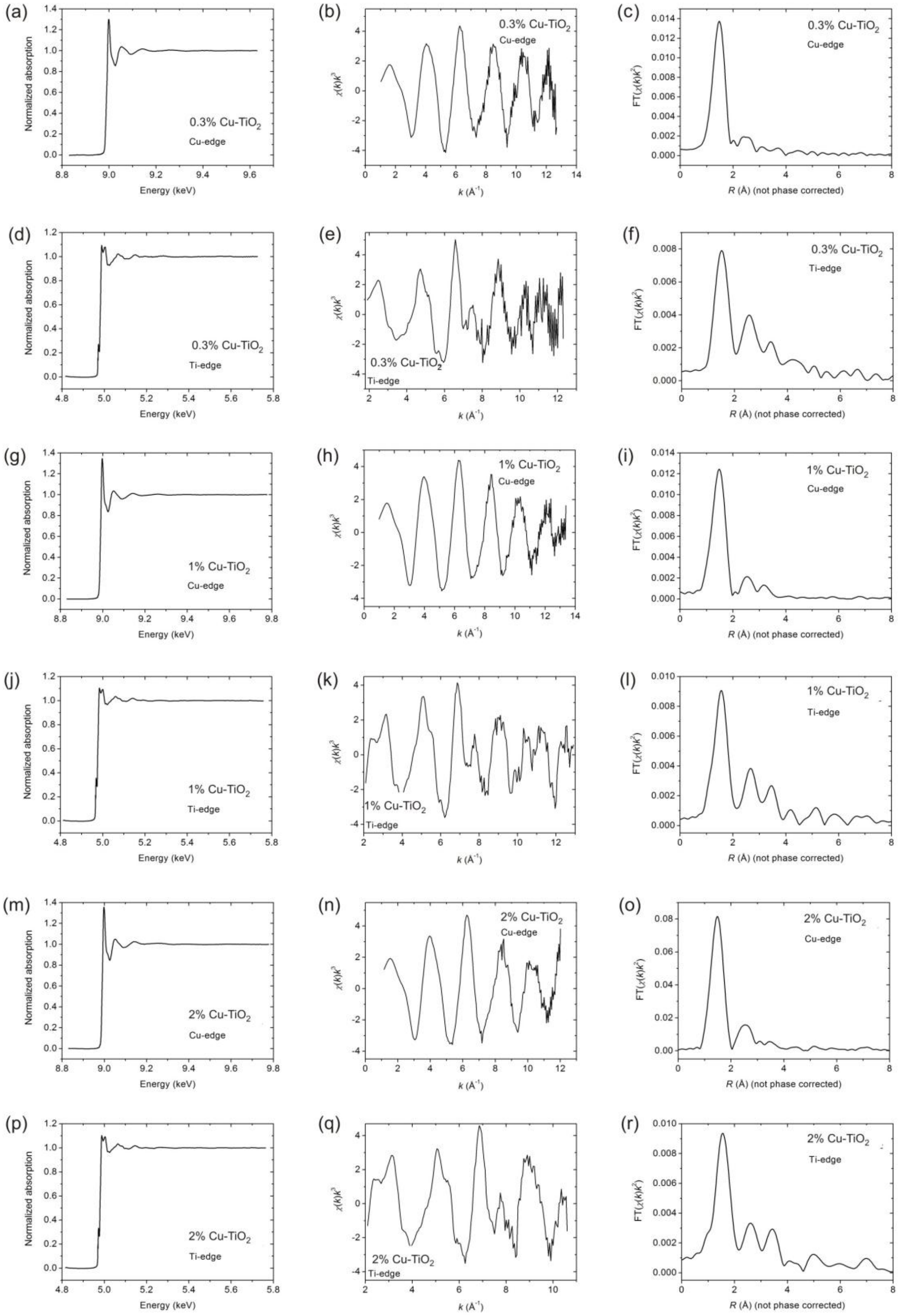

Figure S4. XAS data for Cu-TiO$_2$ displayed as normalized absorption data (1st column), the isolated k^3-weighted EXAFS data (2nd column), and the Fourier transformed EXAFS data (3rd column). (a)-(f) 0.3% Cu-TiO$_2$, (g)-(l) 1% Cu-TiO$_2$, (m)-(r) 2% Cu-TiO$_2$.

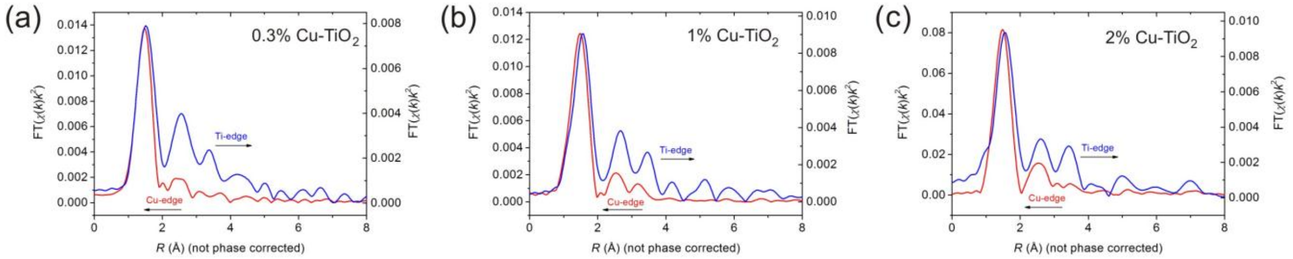

Figure S5. Fourier transformed EXAFS data collected on the Cu-edge (red) and Ti-edge (blue).

Theoretical EXAFS scattering path were calculated for pure anatase TiO_2 and for Cu-TiO_2 with copper at interstitial sites (Model 1) and copper at titanium positions (Model 2) (Table S2-S4). The calculations were based on a CIF file for anatase (no. 154601) from the ICSD database

Anatase TiO_2 (Ti Absorber)			
Scattering path	Degeneration	Amplitude (%)	r_{eff} (Å)
Ti-O_a	4	100	1.941
Ti-O_b	2	49.2	1.955
Ti-Ti_b	4	43.7	3.029
Ti-O_b-O_a	8	12.2	3.173
Ti-Ti_a-O_a	8	12.4	3.463
Ti-Ti_a-O_b	8	12.4	3.463
Ti-Ti_b	4	25.6	3.796
Ti-O_a-O_a	4	14.7	3.839
Ti-Ti_b-O_a	8	46.5	3.839
Ti-O_c	8	39.8	3.855
Ti-O_a-Ti-O_a	4	19.7	3.882
Ti-O_a-Ti-O_a	4	10.3	3.882
Ti-O_a-Ti_b-O_a	4	24.6	3.882
Ti-O_b-Ti-O_b	2	14.1	3.910

Table S2. Theoretical scattering paths with effective bond distances, r_{eff}, up to 4 Å, are shown for anatase TiO_2 (titanium absorber). Only paths contributing at least 10% of the strongest scattering path are included. The paths marked with blue are single scattering paths.

Interstitial Cu in Anatase TiO$_2$ (Cu Absorber) – Model 1			
Scattering path	Degeneration	Amplitude (%)	r_{eff} (Å)
Cu-O$_a$	2	100	1.849
Cu-O$_b$	4	100	2.259
Cu-Ti$_a$	4	100	2.428
Cu-Ti$_a$-O$_a$	8	10.6	3.109
Cu-O$_c$	2	18.8	3.259
Cu-Ti$_a$-O$_b$	8	11.5	3.314
Cu-Ti$_a$-O$_b$	8	11.4	3.321
Cu-O$_d$	4	31.3	3.508
Cu-Ti$_b$	4	37.6	3.620
Cu-Ti$_c$	2	18.2	3.666
Cu-O$_a$-O$_a$	2	11.3	3.698
Cu-Ti$_c$-O$_a$	4	24.5	3.735
Cu-O$_e$	4	25.7	3.786
Cu-O$_a$-Ti$_c$-O$_a$	2	11.5	3.804
Cu-Ti$_b$-O$_b$	8	10.7	3.910
Cu-O$_d$-Ti$_a$	8	21.0	3.939

Table S3. Theoretical scattering paths with effective bond distances, r_{eff}, up to 4 Å, are shown for Cu-TiO$_2$ (copper absorber) for Model 1 with copper at interstitial sites. Only paths contributing at least 10% of the strongest scattering path are included. The titanium EXAFS for this compound will not differ much from the one described by Table S2 due to the low copper concentration. The paths marked with blue are single scattering paths.

Cu at Ti Sites in Anatase TiO$_2$ (Cu Absorber) – Model 2			
Scattering path	Degeneration	Amplitude (%)	r_{eff} (Å)
Cu-O$_a$	4	100	1.941
Cu-O$_b$	2	49.2	1.955
Cu-Ti$_a$*	4	34.9	3.029
Cu-O$_b$-O$_a$	8	11.8	3.173
Cu-Ti$_b$*	4	20.4	3.796
Cu-O$_a$-O$_a$	4	13.7	3.839
Cu-Ti$_b$*-O$_a$	8	33.7	3.839
Cu-O$_c$	8	36.3	3.855
Cu-O$_a$-Ti$_b$*-O$_a$	4	15.7	3.882

Table S4. Theoretical scattering paths with effective bond distances, r_{eff}, up to 4 Å, are shown for Cu-TiO$_2$ (copper absorber) for Model 2 with copper at titanium positions. Only paths contributing at least 10% of the strongest scattering path are included. The titanium EXAFS for this compound will not differ much from the one described by Table S2 due to the low copper concentration, and, furthermore, copper almost have the same scattering power as titanium. The Ti* indicates that the scattering paths were calculated for copper. This gives slightly different amplitudes than if modeled as titanium. The paths marked with blue are single scattering paths.

Gaussian fits to *R*-space EXAFS data are shown in Figure S6. Four Gaussians are used for each dataset. The fits were used to determine the ratio between areas *A*(2)/*A*(1) of peaks at 1.5 Å (*A*(1)) and 2.6 Å (*A*(2)), respectively.

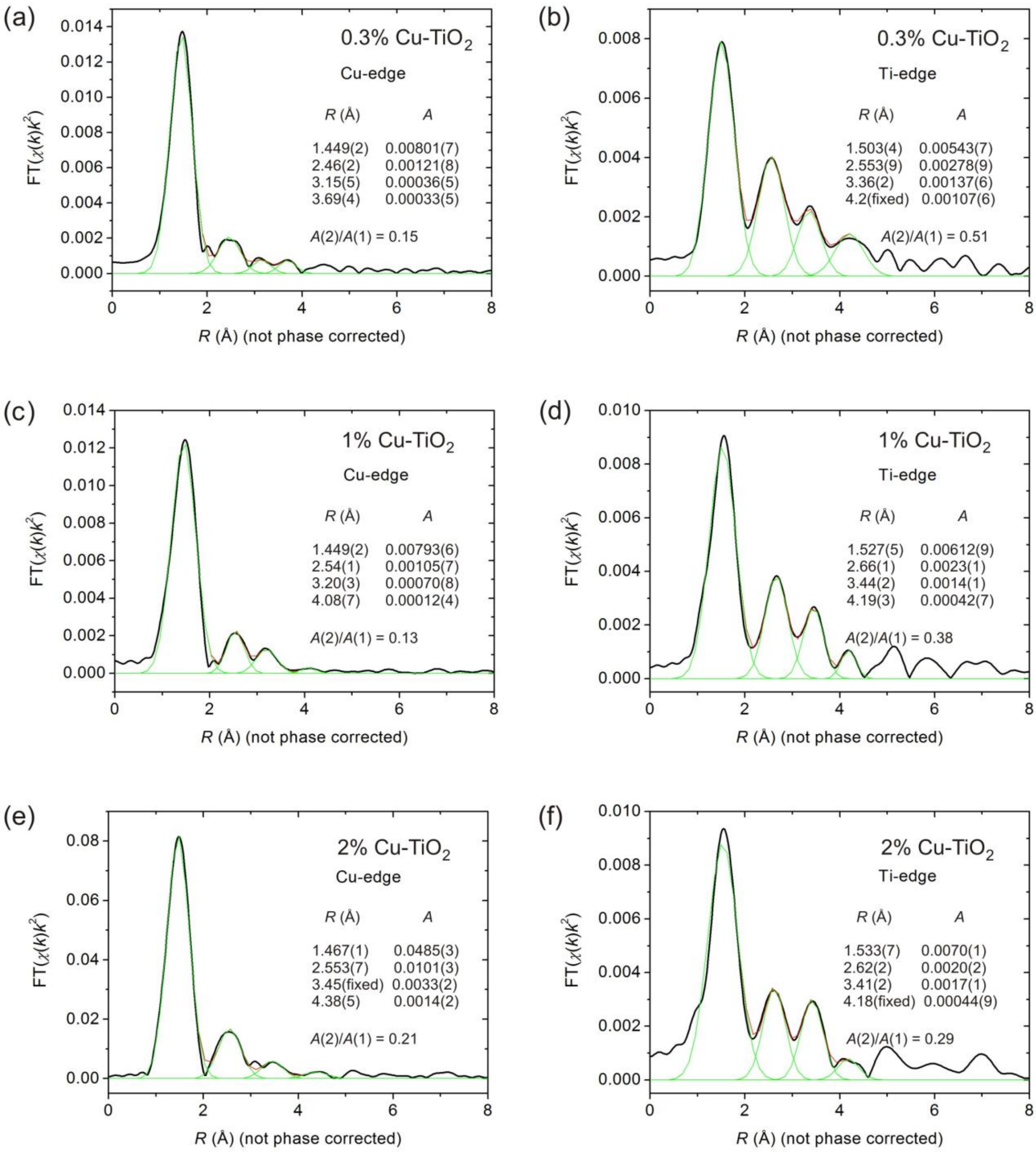

Figure S6. EXAFS data (black) are plotted with Gaussian fits: (a)-(b) 0.3% Cu-TiO_2, (c)-(d) 1% Cu-TiO_2, (e)-(f) 2% Cu-TiO_2. Four individual Gaussians (green) were fitted to data. The sum of the Gaussians is shown as a red line. The positions and peak areas resulting from the Gaussian fitting are displayed, along with the ratio between the areas of the peaks at approximately 2.6 Å (*A*(2)) and 1.5 Å (*A*(1)), respectively.

The titanium- and copper edge data were refined in *R*-space using the WinXAS program.[7] Six scattering path were included in the refinement of the Ti-edge data up to 4.0 Å. All coordination numbers were fixed to their theoretical values (Table S5).

Ti-edge	0.3% Cu-TiO_2			1% Cu-TiO_2			2% Cu-TiO_2		
Path	CN	R (Å)	σ^2 (Å^2)	CN	R (Å)	σ^2 (Å^2)	CN	R (Å)	σ^2 (Å^2)
Ti-O	6	1.940(9)	0.005(2)	6	1.930(6)	0.0030(5)	6	1.939(7)	0.0031(6)
Ti-Ti	4	3.05(1)	0.006(2)	4	3.05(1)	0.005(1)	4	3.06(1)	0.006(1)
Ti-Ti	4	3.91(3)	0.006(2)	4	3.90(2)	0.006(1)	4	3.88(2)	0.002(3)
MS	8	3.85	0.04(2)	8	3.85	0.027(10)	8	3.85	0.024(6)
Ti-O	8	3.85	0.04(2)	8	3.85	0.027(10)	8	3.85	0.024(6)
MS	4	3.85	0.04(2)	4	3.85	0.027(10)	4	3.85	0.024(6)
	E_0 = -1.7(7) eV, S_0^2 = 0.35(5) R =13.9%			E_0 = 11.6(7) eV, S_0^2 = 0.245(9) R =14.0%			E_0 = 12.9(6) eV, S_0^2 = 0.25 R =14.7%		

Table S5. Results of the titanium edge refinements. All parameters without shown uncertainties were fixed in the refinement. Multi-scattering paths have been abbreviated as MS. The Debye-Waller factors of the three scattering paths at 3.85 Å are very high suggesting that the applied model is too simple or that the coordination numbers are lower than their theoretical values. However, these Debye-Waller factors do not influence the analysis of the dopant structure.

The copper edge data were refined (using three scattering paths) against two models: (i) fixed coordination numbers and refined Debye-Waller factors and (ii) refined coordination numbers and fixed Debye-Waller factors. A similar approach was used by Bouchet *et al.*[8] Table 2 in the manuscript sums up the results.

Plots of the refined data are shown in Figure S7 in *k*- and *R*-space (data were only refined in *R*-space). For the titanium edgedata there is a large discrepancy between the *k*-space data and the model. This can be explained by the fact that the applied model does not include scattering paths above 4.0 Å.

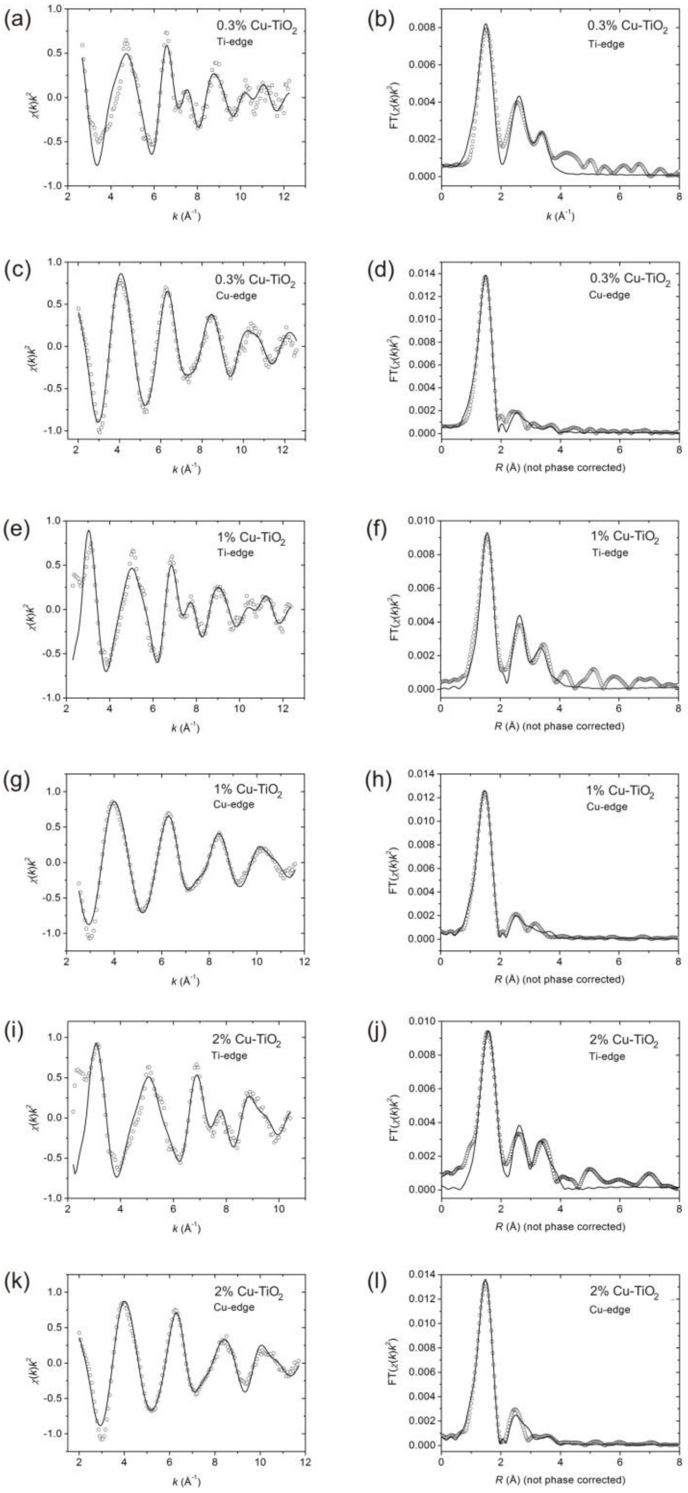

Figure S7. Refined Ti- and Cu-edge data: (a)-(d) 0.3% Cu-TiO$_2$, (e)-(h) 1% Cu-TiO$_2$, and (i)-(l) 2% Cu-TiO$_2$ (data points are shown as grey circles and the model as a black line). All refinements were perfomed in *R*-space *i.e.* the plots in *k*-space are not fits. The copper edge refinements are shown for the model with fixed Debye-Waller factors and refined coordination numbers (model(ii)).

Total Scattering and PDF analysis

Total scattering data were collected at room temperature at beamline 1-ID-C at the Advanced Photon Source (APS), USA on a 41×41 cm^2 General Electric α-Si solid state detector. By using a wavelength of 0.177 Å (70.01 keV) data to a Q_{max} of 28 Å^{-1} were obtained, and full diffraction rings were obtained to a Q_{max} of 21 Å^{-1} on the square detector. Data were measured on an empty polyimide (Kapton) capillary in addition to the Cu-TiO$_2$ sample with the highest copper concentration *i.e.* 2% Cu-TiO$_2$ (packed in a Kapton capillary). Data were integrated in Fit2D[1], and the integrated total scattering data are plotted in Figure S8.

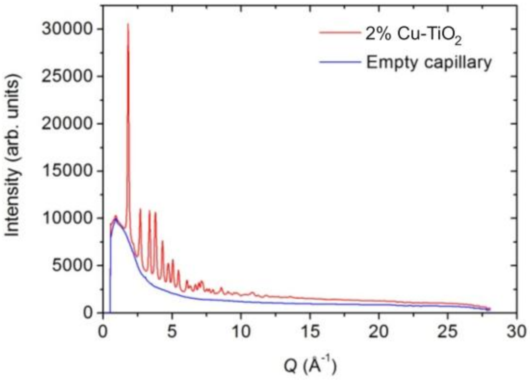

Figure S8. Total scattering data collected on a 2% Cu-TiO$_2$ powder in a Kapton capillary and on an empty capillary. The empty capillary data were used for background correction.

Using data to a Q_{max} of 21 Å^{-1} the PDFgetX2[9] program was used to extract the reduced pair distribution function $G(r)$ (or the PDF), and PDFfit2 was used for the data refinement with the PDFgui interface.[10] A refinement was performed in the distance r range of 3-80 Å without taking copper into consideration, and two models were used to refine data in the range 1-20 Å: (1) Pure anatase that does not take copper atoms into account, and (2) a model in which titanium is partly substituted by copper, and oxygen vacancies are introduced to maintain charge balance as a result of substituting titanium(IV) with copper(II). In both models the occupancies were fixed to fully occupy each Ti(Cu) site, and the atomic displacement parameters (ADPs) were refined isotropically (the copper ADP were constrained to the titanium ADP).

A scale factor and the unit cell parameters were refined, and the *z*-coordinate of oxygen was refined as the only general atomic coordinate. The parameter Q_{damp}, which takes the instrumental resolution into account, was determined by refinement of a standard and fixed in the analysis of the Cu-TiO$_2$ data. In the 3-80 Å refinement, the parameter *delta2* was fixed to a value of 4 Å^2, and the parameter *spdiameter* (*i.e.* the nanoparticle diameter) was refined. For the 1-20 Å refinement the *delta2* parameter was refined freely, while *spdiameter* was kept fixed to the value obtained from the 3-80 Å refinement. Figure S9 shows the refined PDFs (1-20 Å) for the two models. There is no apparent difference between the models (see further the discussion in the manuscript). The 3-80 Å refinement result is displayed in the manuscript (Figure 5a). Parameters resulting from the refinements are shown in Table S6.

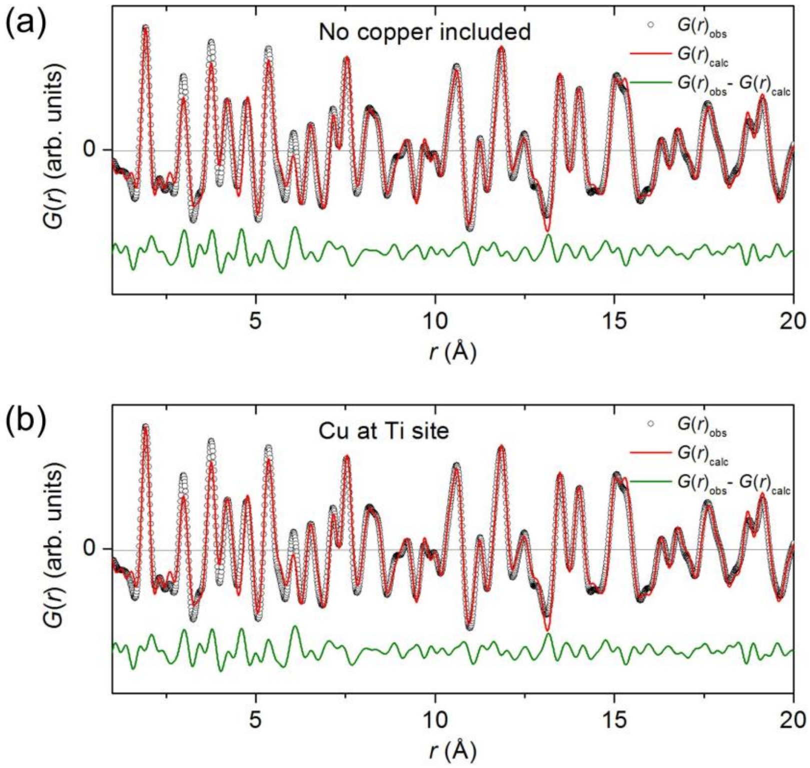

Figure S9. Refined PDF data for 2% Cu-TiO_2 where data are fitted with (a) pure anatase and (b) anatase in which titanium was partly substituted with copper. There is no apparent difference between the fits, which is also reflected in the similar *R*-values of 18.8% and 18.7%, respectively for (a) and (b).

	No copper	No copper	Cu at Ti site
Data range	3-80 Å	1-20 Å	1-20 Å
#(data points)	7701	1902	1902
#(refined parameters)	7	8	8
Q_{damp}	0.02120	0.02120	0.02120
delta2 (Å^2)	4.0	2.6335(5)	2.6425(5)
Scale factor	1.95(2)	1.9628(1)	1.963(1)
a (Å)	3.7433(3)	3.74425(1)	3.74417(1)
c (Å)	9.354(1)	9.34782(2)	9.34812(2)
z(O)	0.1639(2)	0.163633(3)	0.163726(2)
U_{iso}(Ti) (Å^2)	0.0058(1)	0.005393(1)	0.005468(1)
U_{iso}(O) (Å^2)	0.0157(3)	0.015319(4)	0.014975(4)
spdiameter (Å)	55.9(5)	55.9	55.9
R_W (%)	20.5	18.8	18.7

Table S6. Anatase model fitted to *G*(*r*) for 2% Cu-TiO_2.

Powder Diffraction at BL44B2 at SPring-8

Multi-temperature data (300-1000 K) were collected on 0.3% Cu-TiO_2 at beamline BL44B2 at SPring-8, Japan, using a Debye-Scherrer camera. A wavelength of 0.50 Å was used, and the diffracted beam was detected on image plates.

Data were Rietveld refined using the Fullprof software.[2] The background was modelled by linear interpolation of refinable points, and the profile was described with a Thompson-Cox-Hastings pseudo-Voigt function. The 1000 K dataset and the room temperature dataset collected after annealing were described by a rutile phase in addition to the anatase phase. The zero point was fixed to avoid correlation with unit cell parameters, and the profile was refined with the Lorentzian *Y* parameter and two asymmetry parameters. The peak broadening from the instrument was subtracted based on a CeO_2 standard measurement before calculating the particle size. All datasets are displayed in the manuscript (Figure 7a). Examples of refined powder patterns are shown in Figure S10 for the 300 K data (a) before and (b) after heating the sample.

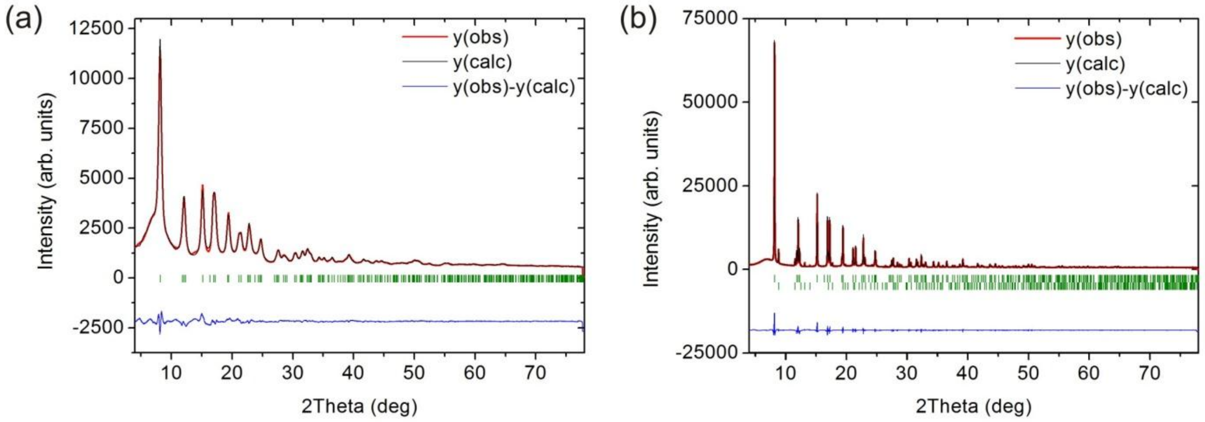

Figure S10. Rietveld refined powder diffraction data from SPring-8 at 300 K (a) before heating and (b) after heating to 1000 K. The broadening at the base of the peak around 10° before heating is the signal from the quartz capillary. The quartz background is also observable in the data after heating, but due to the peak sharpening with heating, its relative intensity is low. Two phases, anatase and rutile, were used in the refinement of the data in (b). The following *R*-values were obtained for the refinements: (a) R_F(anatase) = 2.37%, R_B(anatase) = 2.97%; (b) R_F(anatase) = 4.37%, R_B(anatase) = 3.67%, R_F(rutile) = 13.4%, R_B(rutile) = 11.9%.

Diffuse Reflectance Spectroscopy

Diffuse reflectance spectra were collected on TiO_2 and Cu-TiO_2 in the wavelength range 220-2600 nm covering the ultraviolet (UV), visible, and near infrared (NIR) regions. A thin layer of the dry nanocrystalline sample was spread onto a layer of barium sulphate powder. The reflectance (R) as a function of wavelength was collected in steps of 2.0 nm on a Shimadzu UV-3600 spectrophotometer. The band gap energies of the samples were determined from Tauc plots[11] obtained from the diffuse reflectance spectra as follows.

The data were converted into the Kubelka-Munk function ($F(R\infty)$):

$$F(R\infty) = (1-R)^2/(2R)$$

For an indirect allowed band gap there is the following relation between the Kubelka-Munk function and the band gap energy (E_g). The parameter A is a proportionality constant, and $h\nu$ is the photon energy:

$$(h\nu F(R\infty))^{1/2} = A(h\nu - E_g)$$

The function $(h\nu F(R\infty))^{1/2}$ was plotted as a function of the photon energy ($h\nu$), and the point of inflection was determined as the maximum of the first derivative of the $(h\nu F(R\infty))^{1/2}$ function. The tangent to the inflection point was determined, and the band gap energy was found as the intersection of the tangent with the horizontal axis *i.e.* at $(h\nu F(R\infty))^{1/2} = 0$ (Figure S11).

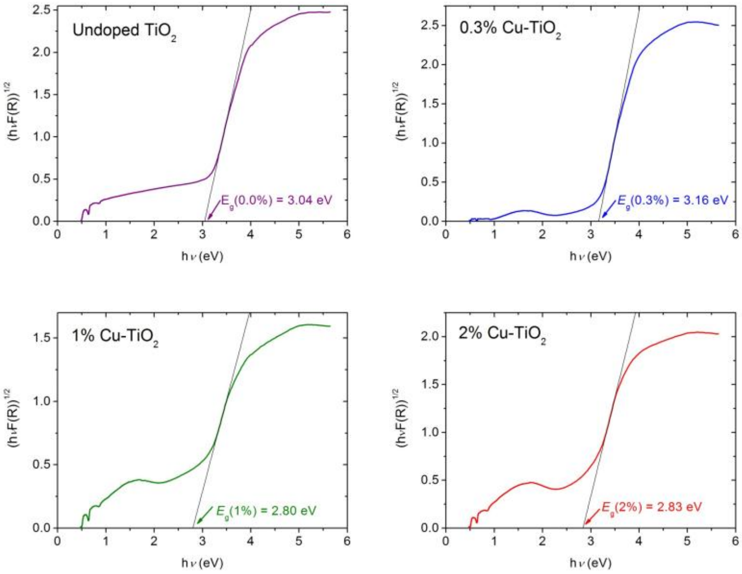

Figure S11. The diffuse reflectance data are represented by the function $(h\nu F(R\infty))^{1/2}$ plotted against the photon energy for the four samples. The band gap energy was determined as the intersection between the inflection point tangent and the horizontal axis at $(h\nu F(R\infty))^{1/2} = 0$.

X-Ray Fluorescence Spectroscopy

X-ray fluorescence (XRF) spectroscopy data were measured on powder samples of the as-synthesized powders on a Spectro Xepos XRF instrument. A standard setting which uses four of the eight available targets was used to determine the copper content in the Cu-TiO_2 nanoparticles. The composition of the samples was determined by using the instrument software. Small sample quantities (approximately 0.1 g) were used for the measurements, and a sample holder with a diameter of 6 or 24 mm was used depending on the available sample quantities. The "loss-of-ignition" values were high when using the 6 mm sample containers (typically approximately 95%), and unexpectedly we found that the determined copper content is dependent on the sample holder size (a factor two between the 6 mm and 24 mm cups) due to systematic errors. Hence, the uncertainty of the absolute copper concentration is high even though it is not reflected in the experimental errors. However due to reproducibility, we believe that the relative copper concentrations for measurements carried out in the same type sample holder are reliable according to the determined 1:2 ratio in copper concentration for the 1- and 2% Cu-TiO_2 (Table S7). Importantly, the absolute copper concentration does not change any conclusions in the paper with respect to the dopant structure, as there were no structural differences between the three studied Cu-TiO_2 samples according to EXAFS data. Due to the low solubility of metal salts in near- and supercritical fluids, we believe that the copper concentrations in the samples should be close to their theoretical values in accordance with the measurement carried out in the large sample holders for the 2% Cu-TiO_2 sample (theoretical concentration: 2.0 wt-%; concentration by XRF: 1.8 wt-%). As the copper content of 1% Cu-TiO2 was determined to 0.55% by XRF in the small cups, we believe the real value is close to 1%, which also corresponds to the synthesis copper concentration.

Sample	Sample holder (mm)	Mass (g)	XRF: Cu (wt-%)	XRF: Ti (wt-%)	Cu-conc in TiO_2 (wt-%)
1% Cu-TiO_2	6.0	0.0631	0.0409(1)	4.322(3)	0.564
	6.0	0.1010	0.04943	5.469	0.539
	6.0	0.0566	0.0424(1)	4.549(3)	0.556
0.3% Cu-TiO_2	6.0	0.0738	0.01127(5)	4.323(3)	0.156
	24	1.415	0.2784(7)	55.89(4)	0.298
2% Cu-TiO_2	6.0	0.0710	0.0673(1)	4.093(3)	0.976
	6.0	0.0611	0.0607(1)	4.235(3)	0.852
	24	0.3787	1.768(2)	58.66(4)	1.78
	24	0.532	1.864(2)	60.99(4)	1.80

Table S7. Details on the X-ray fluorescence spectroscopy measurements. The copper and titanium concentrations in wt-% were evaluated by the instrument software. The reason for the low apparent titanium concentration in wt-% is the high loss-of-ignition (for the 6.0 mm sample holder measurements).

1 A. P. Hammersley, S. O. Svensson, M. Hanfland, A. N. Fitch and D. Hausermann, *High Press. Res.*, 1996, **14**, 235.

2 J. Rodriguez-Carvajal, *Physica B*, 1993, **192**, 55.

3 J. Rodriguez-Carvajal, An Introduction to the Program Fullprof 2000 (Fullprof Manual)

4 B. Ravel, *J. Synchrotron Rad.*, 2001, **8**, 314.

5 J. J. Rehr and R. C. Albers, *Rev. Mod. Phys.*, 2000, **72**, 621.

6 B. Ravel and M. Newville, *J. Synchrotron Rad.*, 2005, **12**, 537.

7 T. Ressler, *J. Synchrotron Rad.*, 1998, **5**, 118.

8 R. Bouchet, A. Weibel, P. Knauth, G. Mountjoy and A. V. Chadwick, *Chem. Mater.*, 2003, **15**, 4996.

9 X. Qiu, J. W. Thompson and S. J. L. Billinge, *J. Appl. Cryst.*, 2004, **37**, 678.

10 C. L. Farrow, P. Juhas, J. W. Liu, D. Bryndin, E. S. Bozin, J. Bloch, T. Proffen and S. J. L. Billinge, *J. Phys.: Condens. Mater.*, 2007, **19**, 335219.

11 J. Tauc, R. Grigorovici and A. Vancu, *Phys. Stat. Sol.*, 1966, **15**, 627.